Editors' Suggestion

High voltage dc gun for high intensity polarized electron source

Erdong Wang,[*,†] Omer Rahman,[†] John Skaritka, Wei Liu, Jyoti Biswas, Christopher Degen, Patrick Inacker, Robert Lambiase, and Matthew Paniccia

Brookhaven National Laboratory, Upton, New York 11973, USA

(Received 12 December 2021; accepted 7 March 2022; published 24 March 2022)

The high intensity polarized electron source is a critical component for future nuclear physics facilities. The electron-ion collider requires a polarized electron gun with higher voltage and higher bunch charge compared to any existing polarized electron source. At Brookhaven National Laboratory, we have built an inverted high voltage direct current (HVDC) photoemission gun with a large cathode size. We report on the performance of GaAs photocathodes in a high gradient with up to 16 nC bunch charge. The measurements were performed at a stable operating gap voltage of 300 kV—demonstrating outstanding lifetime and robustness. We observed obvious lifetime enhancement by biasing the anode. The gun also integrated a cathode cooling system for potential application on high current electron sources. The various novel features implemented and demonstrated in this polarized HVDC gun will open the door toward future high intensity-high average current electron accelerator facilities.

DOI: 10.1103/PhysRevAccelBeams.25.033401

I. INTRODUCTION

The electron-ion collider (EIC) at Brookhaven National Laboratory (BNL) will be colliding polarized electrons with polarized hadrons to probe into various unsolved mysteries of nuclear physics [1]. In order to achieve the expected luminosity of the collider, a high bunch charge, high intensity polarized electron source is required [2]. The polarized electron source should be able to provide 5.5–7 nC per bunch in a bunch train structure with eight bunches every second. To achieve the required beam qualities before injecting the beam into the rapid cycling synchrotron (RCS) and minimize beam loss, the gun voltage has to be above 280 kV with beam peak current above 4.5 A according to the current preinjector design [3]. This gun will have to provide at least two weeks of continuous operation before the cathode can be exchanged.

There have been substantial efforts in high voltage polarized gun development in the last few decades. The Stanford Linear Collider (SLC) gun has demonstrated extraction of up to 12 nC bunch charge at 120 Hz. The gap voltage for the SLC gun was 120 kV and the cathode had to be reactivated every 3–5 days [4]. JLab Continuous Electron Beam Accelerator Facility (CEBAF) gun operates at < 10 pC bunch charge with gap voltage up to 200 kV. Cathode operational lifetime at CEBAF is over a month for 200 μA average beam current operation [5]. Until now, all the polarized guns have operated at a gap voltage less than 200 kV to eliminate field emission [4,6–12]. On the peak current aspect, SLC and Nagoya dc guns have achieved 2–6 A of peak current. However, the rest of polarized guns have peak currents up to tens of mA range. So far, no operational or retired polarized gun can fully meet the EIC polarized electron source requirements.

At BNL, we have developed a high intensity polarized electron gun based on an inverted high voltage feedthrough design with a higher gap voltage and large cathode size. The cross-sectional view of the BNL gun is shown in Fig. 1. This gun can consistently operate at 300 kV gap voltage without any detectable field emission. The following features have been implemented into the gun to generate high intensity polarized electron beam: (1) Inverted high voltage (HV) feedthrough to minimize outgassing area; (2) ceramic feedthrough and two triple-point shields to minimize the electric field gradient at the ceramic-vacuum-metal joint and linearize the voltage along the length of the ceramic; (3) movable and electrically insulated anode; and (4) a HV cable with a slightly conductive jacket, which prevents charge buildup, but does not deliver energy to an arc as a conductive shield would. Moreover, for future high current applications, we have developed a cathode cooling system integrated into the high voltage feedthrough in the gun. These novel features can be applied in future polarized electron\positron sources and high brightness high current electron sources, to be used for future scientific user facilities, such as the large hadron-electron collider at the High-Luminosity Large Hadron Collider, polarized

[*]Corresponding author.
wange@bnl.gov
[†]E. W. and O. R. contributed equally to this work.

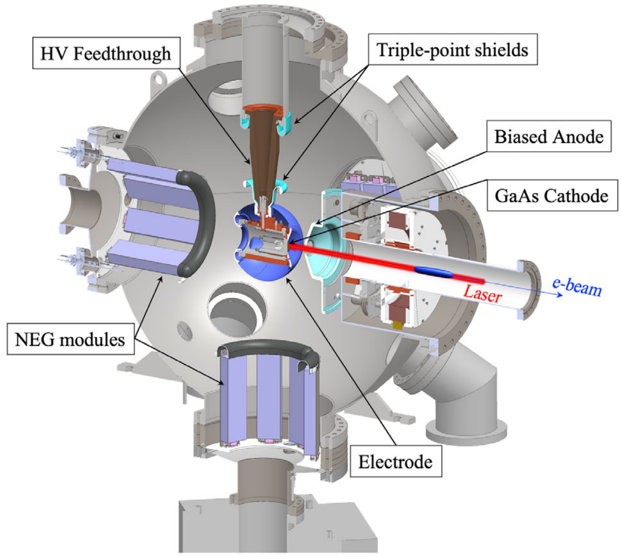

FIG. 1. Cross-sectional view of the BNL HVDC gun.

positrons experiment, strong hadron cooling or energy recovery Linac based light sources [13–18].

In this article, we report on our high voltage direct current (HVDC) gun design, gun performance including high voltage and vacuum performance, space charge limit, and lifetime measurements with 7.5 nC bunch charge.

II. INVERTED HVDC GUN DESIGN CONSIDERATIONS

For an HVDC gun to deliver high intensity polarized electron beam with a good operational lifetime, a few considerations are critical during the inception stage. These considerations are implemented to prolong charge lifetime by minimizing cathode quantum efficiency (QE) decay rate, while delivering high intensity beam with good quality and minimal loss. The cathode QE is determined by the photon energy $h\nu$, band gap E_g, and surface electron affinity E_a. GaAs photocathode is a direct band gap semiconductor. To produce high polarization electron beam, the cathode has to be operated in threshold photoemission mode, i.e., photon energy $h\nu \approx E_g$, which results in QE being very sensitive to the degradation of the activation layer [19]. Any contaminations on the cathode surface will increase E_a, which in turn lowers the QE. To extend cathode long lifetime, the following effects have to be considered while designing the gun.

(1) *Ultrahigh vacuum*. The GaAs cathode emission surface is coated by a O(NF3)-Cs which is very sensitive to gas contamination including methane, carbon monoxide, carbon dioxide, oxygen, water, and other active gases [20]. The active gases degrade the quantum efficiency (QE) by chemical poisoning or via ion back bombardment. Thus to obtain a long lifetime, the gun chamber dynamic pressure should be in 10^{-12} Torr scale with hydrogen being the dominant gas (above 99% of the gas load) [5,21].

(2) *High voltage*. For high bunch charge beam, high gradient and high voltage are desirable on the cathode. However, the gradient cannot exceed 10 MV/m to avoid field emission. Depending on the desired bunch charge, the cathode size could be determined so that an adequately sized laser spot can be used to avoid the space charge limit and surface charge limit. To avoid the field emitted electrons punching through the ceramic, an appropriate shield should be designed to protect the ceramic feedthrough [22].

(3) *Beam loss*. The beam loss close to the gun will cause an increase in the dynamic pressure. The main source of beam loss is from the beam halo. Therefore, a large beam pipe at the exit of the gun is necessary to minimize the effect of beam loss [23].

(4) *Ion back bombardment*. Ion back bombardment could be a dominant mechanism that limits the cathode lifetime. Although ion back bombardment from ions generated in the dc gap cannot be eliminated, a biased anode is very useful in eliminating ions that are generated downstream [24–26].

(5) *Masking of cathode active area*. Electrons emitted from the edge of the cathode can take extreme trajectories due to strong transverse kick. Also, electron beam halo (caused by the laser transverse halo) can end up hitting the wall and create outgassing. Thus, the emission area should be kept at a safe distance from the edge of the cathode [27,28].

We chose the load-lock inverted feedthrough as our gun type. Since one side of the inverted HV feedthrough is in a vacuum and another side is in contact with silicone grease and rubber, it minimizes the creepage compared to the case when the ceramic is exposed to the atmosphere. Therefore, the ceramic feedthrough size can be reduced which will result in a compact chamber design. This structure also eliminated the field emission electrons hitting the ceramic feedthrough [29]. The compact chamber reduces the outgassing surface area and results in ultrahigh vacuum in the chamber with sufficient pumping. With the cathode load-lock system, the cathode can be activated at a separate preparation chamber, other than activating in the gun chamber such as SLC gun or JLab-FEL HVDC gun [4,30]. A cathode load-lock system is used to permit the exchange of the photocathode within an hour.

A large cathode with a sufficiently large laser spot size can generate a high peak current electron beam. However, too large of a cathode size will drastically increase the overall cost of the vacuum components. For this gun, the cathode size was designed to be 1.26 cm in radius so that the cathode puck can be transferred through a 4.5 in. all-metal valve. The bunch charge of 7 nC cannot be a pancake shape from a dc gun which has a gradient on the cathode to be less than 5 MV/m. The space charge limit for the pencil shape beam is

$$J_{2d} = 2.33 \times 10^{-6} V^{3/2}/d\left(1 + \frac{d}{4r}\right), \tag{1}$$

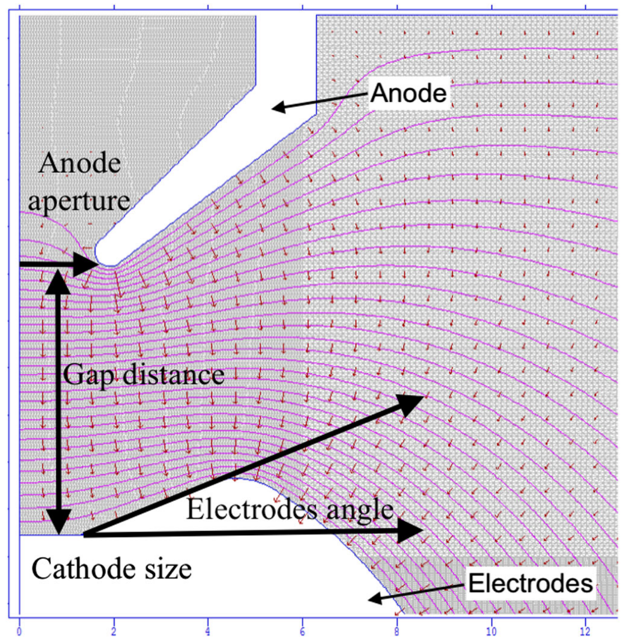

FIG. 2. dc gap geometry and field distribution. The optimized parameters are listed.

where V is the voltage across the dc gap distance d and r is the laser spot size radius [31]. The gap distance is determined by the maximum gradient on the electrode which has to be less than 10 MV/m to avoid field emission. Higher gap voltage can increase the surface charge limit. The commercially available inverted feedthrough R30 can hold high voltage up to 400 kV [32]. We designed our gun voltage up to 350 kV. Having higher voltage has the following advantages: (1) Can generate high charge beam with high peak current by increasing the space charge limit; (2) eliminate the surface charge limit by lowering the surface barrier [33,34]; and (3) preserve the beam longitudinal and transverse emittance during ballistic compression in the injector. The EIC preinjector baseline design shows that to achieve 7 nC bunch charge from a 300 kV gun with minimum emittance and energy spread, the peak current is 4.5 A, the FWHM bunch length is 1.6 ns, and beam size is 8 mm [2,3]. To get minimal required beam quality before injecting beam into the RCS, the gun operational voltage has to be above 280 kV. It is conservative compare to our design voltage.

The dc gap and high voltage components in the gun were optimized to get small emittance and minimize the maximum surface gradient of the negative potential metal components. The optimization constrains are the following: (i) The gradient on the −350 kV metal parts has to be less than 10 MV/m; (ii) the gun electrode ball size has to be less than 20 cm in diameter to fit into the chamber flange and barrel polishing machine; (iii) the cathode puck size has to be less than 4.5 cm in diameter, limited by the all metal valves aperture; (iv) the size of GaAs exposed to the high voltage has to be larger than 2.4 cm in diameter to allow up to a 6 mm diameter off-centered laser placed in the linear field range; and (v) the anode opening has to be larger than cathode size to utilize the entire cathode without clipping the laser or beam loss from the cathode edges. The Pierce-like geometry was optimized by achieving small emittance after space charge compensation downstream of the first solenoid. The optimal parameters are the cathode size, electrodes angle, gap distance, and the ratio of Pierce focusing size to the cathode size as shown in Fig. 2. The anode aperture size is set to 1.4 times of the cathode size to make sure that the stray beam from the laser transverse halo or scattered photons can be extracted from the gun without any loss on the anode. The cathode size and electrodes angle were scanned in the range of 2.4–3 cm, and 20° to 30°, respectively. The anode cone slope is parallel with the electrodes cone shape. The gap distance was tuned to get maximum field gradient on the Pierce nose equal to 9.5 MV/m. The optimized gun geometry parameters and simulated beam quality parameters are listed in Table I.

TABLE I. dc gun design parameters.

	Value
Gap voltage	350 kV
Cathode radius	1.26 cm
Electrodes angle	22°
Gap distance	5.6 cm
Cathode gradient	3.8 MV/m
Maximum gradient on the electrodes	9.4 MV/m
Anode radius	1.8 cm
Peak current	4.5 A
Bunch charge	7 nC
Normalized emittance	3.4 mm mrad

III. HIGH VOLTAGE PERFORMANCE

Once the electrode and anode geometries were optimized for the best possible beam quality, the next considerations are the following components: high voltage feedthrough, triple-point shields, anode shape, and nonevaporable getter (NEG) pump positioning. We used a 90 cm diameter spherical chamber as the gun chamber, with a 20 cm diameter spherical electrode to reduce the surface gradient. The HV feedthrough used for this gun is carbon-doped alumina which allows trapped electrons on the ceramic surface to be removed [35].

The high voltage section's geometry was designed using POISSON and OPERA3D and the field gradient is shown in Fig. 3 [36,37].

At 350 kV gap voltage, the maximum gradient of 9.4 MV/m occurs at the cathode Pierce shape nose (labeled 1) and the triple point shield (labeled 3) as shown in Fig. 3. The gradient at the center of the cathode surface is 3.8 MV/m. The cathode linear field range is up to 9 mm in radius. Therefore, we

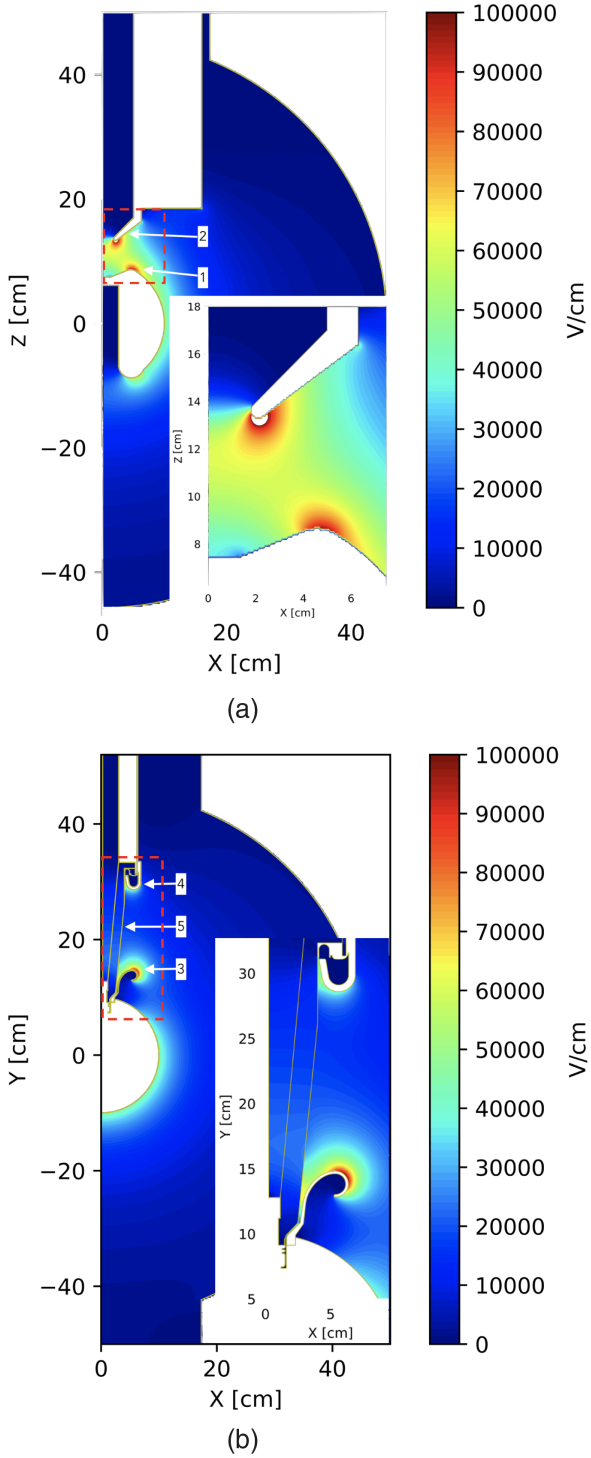

FIG. 3. The field gradient of the HVDC gun. The most important parts as dashed red boxed are zoomed in. The main high gradient locations are labeled: 1: Pierce nose; 2: anode; 3: HV trip-point shield; 4: grounded trip-point shield; and 5: ceramic. (a) The field gradient map on the dc gap. (b) The field gradient on the HV ceramic feethrough.

can offset the laser 9 mm or with a large laser size of 9 mm in radius with increasing initial normalized emittance no more than 25% [26].

The triple point is a metal-ceramic-vacuum interface point that usually has a local maximum of the field gradient. Two triple-point shields were optimized and designed to minimize the gradient on the triple point and to generate a linear potential along the feedthrough to avoid electron trapping as shown in the Fig. 4 red curve. The gradient at the triple point on the electrode side reduced to less than 1 MV/m, while the gradient at the ground side reduced by half compared to without triple-point shield as shown in the Fig. 4 blue curve. The 30 MV/m gradient on the ground side triple point is still high. However, the shield is less than 1 mm away from the ground at this position, resulting in electrons getting absorbed by the shield instead of reaching the ceramic feedthrough. The transverse size of the triple-point shield is determined by the transverse kick that it imparts on the electron beam. In our design, the deviation of the beam's trajectory from the cathode to the first corrector coil is less than 0.5 mm.

We combined the mechanical polishing and superconducting radio frequency particulate cleaning process for our high voltage components. The stainless steel electrode and triple-point shields were polished mechanically using a tumbler for an hour, following the method developed by JLab [38]. The titanium anode was mechanically polished at a vendor using alumina powder. Then, the electrode, triple-point shields, anode, and the ceramic were ultrasonic cleaned to remove residual surface contaminants and polishing media. Then high pressure rinsing was performed on all metal parts with 1400 psi for 3 h and 300 psi on ceramic for 3 h, then we dried them in a class 10 clean room overnight for preassembly. All the gun and beam line final installation was carried out in a class 100 clean room.

We used a Glassman high voltage power supply (HVPS) at a maximum of 400 kV. It can provide a maximum current of 6 mA at this voltage. To avoid the use of environmentally adverse sulfur hexafluoride (SF_6) or oil, the power supply is in air within a grounded cage. This places the HVPS about

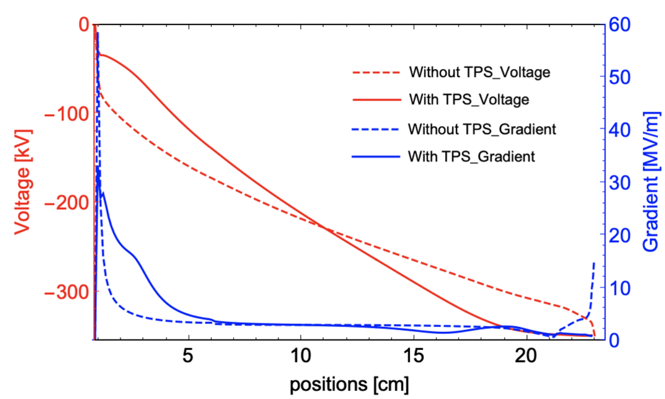

FIG. 4. The potential and gradient along the ceramic feedthrough, comparison between with and without triple-point shields (TPS). The position 0 cm is the ground side of the feedthrough, toward the 24 cm of high voltage electrode side.

5 m from the gun. If there is an arc during the beam operation in the dc gap, the stored energy in the cable (which at 50 pF/ft is about 46 J) will damage the polished electrode. To avoid this from happening, we used a semiconducting layer as the shield of the cable with a resistivity of 10^{10} ohm cm. The resistivity is low enough to keep the cable from building charge but high enough to limit the delivery of stored energy from the cable in the dc gap. During conditioning, external 100 MΩ resistors were used in series, between the power supply and gun, to avoid damage to the polished electrode by a strong discharge.

We installed a cathode puck with a GaAs wafer to condition the gun. The gun achieved 350 kV gap voltage after about 21 h of conditioning. A few field emitters were found during the voltage ramp-up, however, none of them were so-called hard barriers that required more than 5–6 h of vacuum conditioning. The trip limit for the power supply was set to 300 μA, which was never reached during the conditioning process. A power over fiber (POF) system was used to measure the current in the dc gap during gun conditioning. The maximum discharge we observed via POF measurement is about 120 μA, which occurred at 210 and 350 kV and generated 10^{-8} Torr vacuum spikes. We did not have to use any inert gas, such as helium or krypton, for this conditioning process to achieve the design voltage. Vacuum excursions up to high 10^{-8} Torr were observed during the conditioning process, however, the vacuum in the gun could recover within the next few minutes after such excursion. We stopped to pursue even higher voltage because the electrode maximum gradient already reached 10 MV/m. Four Geiger counters were placed around the gun during the conditioning process.

During the gun conditioning, we increased the voltage in small increments (1 kV per step) and monitored the POF current, vacuum, and Geiger counter readings. The discovery of a field emitter was generally sudden. This is why the current limit was set to 300 μA to limit the energy deposited in the gun during a discharge event. Once the field emitter was found, we waited at that voltage level for the field emission current to gradually decrease to a level that we were comfortable with (generally below 50 μA). We also ensured that the vacuum level was not at 10^{-8} Torr level for a long period of time, for example more than 30 min. Once the current has decreased to below that level and the vacuum has recovered, we would slowly increase the voltage by 1–2 kV every 5 min to increase the current slightly such that the conditioning process was expedited. For example, at around 210 kV, as shown in Fig. 5, we observed a sudden onset of a field emitter accompanied with a 100 μA current spike and vacuum spike up to 3×10^{-8} Torr scale. However, the current dropped to about 1 μA within a couple of minutes, while vacuum dropped to low 10^{-10} Torr. In that particular instance, we continued ramping the voltage slowly up to 250 kV for the next several hours since POF current was below our predetermined threshold of 50 μA and vacuum was at 10^{-9} Torr scale. Then around 250 kV, we had another large current spike over 100 μA, and therefore, we continued with the same strategy as mentioned above. We achieved 315 kV in about 18 h, then back to 300 kV for 2 h. No field emitter was observed. We ramped the voltage up until we observed the field emission at 340 kV, which was conditioned in a couple of hours and the final achieved voltage was 350 kV. Note that conditioning up to this point was done with an unactivated GaAs puck. Subsequently, we used a Cs–O activated GaAs to repeat this experiment, and we could achieve 350 kV without any field emission.

After the gun was conditioned up to 350 kV, the Geiger counters and field emission current showed background noise, and the vacuum got into 10^{-12} Torr scale. Figure 5 shows the overall conditioning time along with the current, vacuum, and averaged radiation levels in the gun. Our total high voltage conditioning duration is much shorter than other comparable HVDC guns, indicating our new

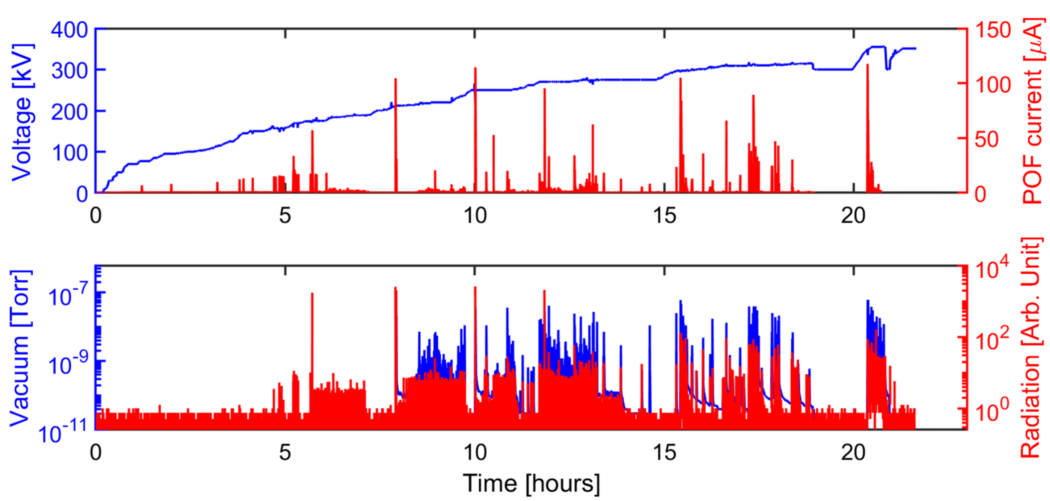

FIG. 5. HVPS conditioning process to reach 350 kV.

posttreatment and clean processing might have played an important role [29,39,40].

There were instances where we extracted a used puck from the gun, transported it to load-lock chamber, and eventually exposed it to atmosphere to change the GaAs substrate. Once the "fresh" cathode was inserted into the gun, without any activation (just heat cleaning), we observed field emission around 325 kV which could be conditioned easily. This indicates that this field emitter might have appeared since this puck was not high pressure rinsed and it might have had some particulate on it. Once this fresh cathode was conditioned, 350 kV voltage could be achieved easily with or without an activated layer. Achievement of 350 kV with an activated cathode indicates that the gun's operating voltage did not get affected by the activation layer. The field emitters from fresh cathodes are merely an artifact of the cathode substrate exchange process which can be improved upon, for example, by having every puck high pressure rinsed. To avoid any chance of field emission during operation, we operated the gun at 300 kV with a sufficient safety margin.

The field emission current at 300 kV was lower than the noise, checked by the electrometer connected to the anode and current measurement from the POF system. We did not observe any QE drop overnight when the cathode was at 300 kV voltage without beam. 300 kV operational voltage for this polarized gun is already higher than any other, existing or retired, polarized electron source [6,11].

IV. CATHODE HEAT TRANSFER

The gun was originally designed for mA scale average current operation [41]. Because the EIC changed the collider scheme and the electron source project changed the scope, our laser, machine protection system, and the beamstop limited us to pursue average current beyond 70 μA. However, in the gun design and fabrication stage, we already implemented a cathode cooling system to avoid the cathode overheating by the incident laser power in high current operation [22].

The gun side of the cable end is a modified, spring-loaded, R30 type plug. This modification was made by machining a pair of spiral grooves in the plug to accommodate the flow of Fluorinert (FC72) to the tip of the plug for heat exchange and then back. The spring loading provides good contact between the plug and ceramic feedthrough to maintain FC72 flow in the cooling channel. A flow rate of greater than 0.5 gallons per minute is used, which does not result in cavitation. A chiller is used to maintain the FC72 fluid at room temperature. This specialized cable, inserted into the R30 ceramic feedthrough, was successfully tested at the Dielectric Sciences facility at up to 415 kV in SF_6. The schematic drawing of the modified plug integrated into the HV feedthrough design is shown in Fig. 6.

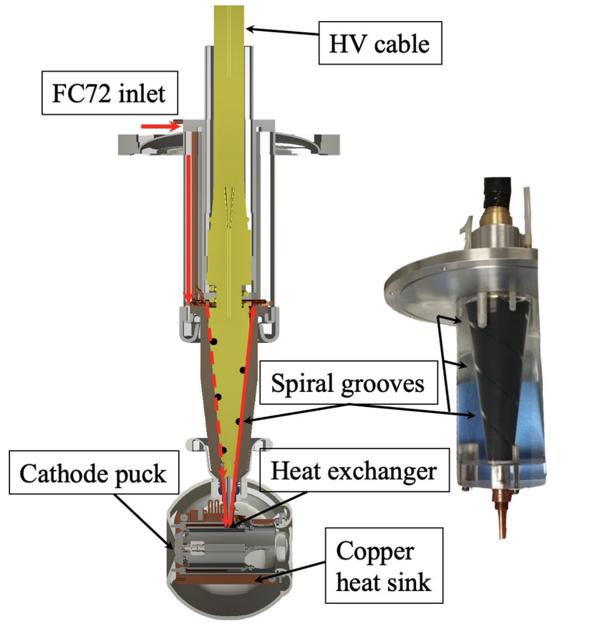

FIG. 6. The left figure is the cross view of the modified plug with the HV feedthrough and electrodes. The FC72 flow path is shown in red arrow. The right figure is the picture of the modified plug in a transparent acrylic container to test the grease uniformity.

FC72, due to its low viscosity, is known to be a fluid that is difficult to seal. MIT-Bates developed a cooling channel mechanism to cool the cathode. However, they faced a major problem of FC72 leaking into the vacuum system [42,43]. To ensure that there were no leaks into our vacuum system, we used continuous flow paths without decouplable mechanical joints in the FC72 flow path. Our residual gas analyzer (RGA) did not pick up any characterizing signal of FC72, showing that we had no leak into the system.

After assembling the cable plug into the ceramic and filling up the FC72 in the cooling loop, we occasionally observed air bubbles coming out from the plug due to gas trapped in the nonuniformity of the grease coating. This process will be mitigated by itself by redistributing the grease in about 12 h of continuous circulation until there are no bubbles in the tube. Cameras are set up to monitor the flow paths for bubbles. We also found that a continuous FC72 flow can dissolve the silicon grease and can leave grease residue in the return tube. The grease residue will change the cooling flow rate and result in degrading the cooling capability, therefore recoating grease on the plug and cleaning the cooling loop have to be carried out every 3 months.

This setup has successfully operated the continuous FC72 flow more than a year without any leaks. We did not observe any failure in more than 500 h of operation at high voltage ($\geq$ 300 kV). A preliminary heat transfer test was carried out using this setup. The cathode temperature was seen to rise up to 60 °C when 10 W of power was applied on the surface of the cathode without any cooling. Once the FC72 flow was implemented through the cooling channel, the cathode temperature dropped to 15 °C. In principle, it also can be used for high current unpolarized electron source—the multialkali cathodes such as K_2CsSb can survive at this temperature when 100 mA of average current is being generated, with laser power less than 10 W if the QE is above 2.3% [44].

V. GUN TEST BEAM LINE

We developed a gun test beam line, for this gun, as shown in Fig. 7. Five solenoids maintain the beam envelope until the beam is delivered to the beam dump. A 16° bending dipole is placed after the second solenoid. The dipole magnet prevents the charged particles from downstream from tracing back to the gun and also can be used for measuring the beam energy. The circularly polarized laser is delivered to the cathode, normal to the cathode surface, through the dipole chamber. The normal incidence of laser to the cathode surface is necessary to get high polarization.

One fast current transformer and one integrated current transformer (ICT) are used to measure the bunch length and bunch charge. Four yttrium aluminum garnet (YAG) beam profile viewers are installed in the beam line to measure the beam transverse profile from the gun to the beam dump. The first YAG crystal has a 9 mm diameter aperture in the center, therefore the incident laser can pass through the viewer without scattering. It also can be used to measure beam halo. Two four-button beam position monitors are used to monitor beam positions before and after the dipole during the operation. The aperture of the beam pipe is 10 cm in diameter which is 10 times the maximum root mean square (rms) beam size for 5 A peak current. The space charge beam tracking simulation shows that beam halo in our case can be well accommodated until it reaches the beam dump [22]. The planned differential pumping stages are not installed at this moment due to the change in the project scope.

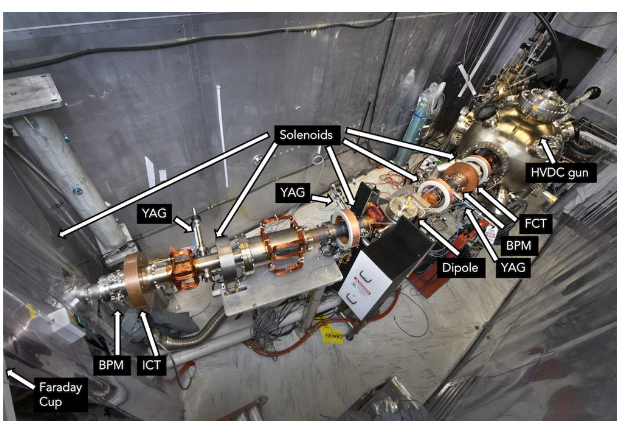

FIG. 7. The HVDC gun test beam line. All the diagnostics are labeled.

VI. GUN AND BEAM LINE VACUUM

For the polarized electron source and beam line, a 10^{-12} Torr scale vacuum is required. In our system, the pumps in the gun area combine a sputtering ion pump and 8000 L/s nonevaporation getters (NEGs) with ZAO material [45]. We performed a Monte-Carlo simulation using MolFlow+ to estimate the pressure on the cathode surface and optimize the gun vacuum design [46]. Figure 8 shows the pressure distribution in the chamber from MolFlow+ simulation, assuming beam induced outgassing at the beam dump. The beam line dynamic vacuum is typically worse than the pressure in the gun. To prevent the backstreaming molecules from reaching the cathode through the anode aperture, we designed a gap between the anode and vacuum chamber to provide extra vacuum conductivity. This will help in intercepting the gas coming from downstream before it reaches the cathode.

The choice of gun material and postprocessing are crucial for achieving ultrahigh vacuum and high voltage. We chose the vacuum remelt cross forged 316LN as our HV electrode material because it can achieve good smoothness due to its fine crystal. It was hydroformed, welded, and fired up to 930 °C for 4 h to demagnetize and degas the diffused hydrogen in the material. The gun chamber and all the gun flanges were also vacuum fired up to 930 °C for 4 h to reduce the diffused hydrogen. Then the knife edges were machined. The thickness of the various stainless steel components, as applicable, was reduced to 5 mm to minimize the gas load after vacuum firing. The anode is made out of titanium due to its low atomic number. This will

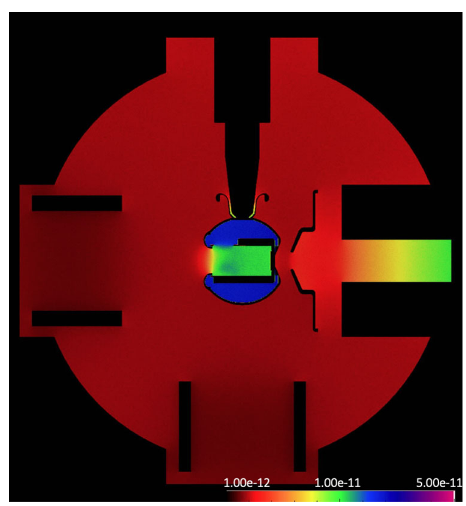

FIG. 8. The dynamic vacuum distribution in the gun chamber. In the simulation, we assume the stainless steel outgassing rate is 5×10^{-13} mbar L/s/cm^2. The beam dump pressure was assumed to be 1×10^{-8} mbar for this simulation.

minimize the generation of x rays when the field emission electron beamstops on the anode during gun conditioning. We also use a larger anode size, 32 cm in diameter, compared to other existing guns. The field emission from the highest gradient position, as shown in Fig. 3, will stop on the titanium anode, other than the stainless steel chamber to further reduce x rays. The anode is mounted on three electrically insulated actuators which provides flexibility to fine-tune the anode position (in both longitudinal and transverse directions) and to be able to bias or use as a current pickup. The longitudinal movement can be used to optimize the voltage and optics in operation, while the transverse movements can be used for further extending cathode lifetime as proposed in Ref. [26]. In this paper, we describe the experiments with the anode positioned at the center of the cathode, with gap distance as shown in Table I. The entire gun assembly was oven baked up to 350 °C for 6 days for final outgassing.

After activating all NEG pumps, the baseline vacuum was 7×10^{-12} measured by the bent belt beam gauge (3BG) [47]. During the beam test, we turned off the 3BG because its hot filament will generate photons, which will in turn generate unwanted electron beam. The RGA measurements performed at the end of the bake showed partial pressure for all gas species to be lower than 10^{-1} (RGA noise level) Torr, except for hydrogen which had a partial pressure of 4×10^{-12} Torr. The dynamic vacuum of the gun, beam line, and beam dump will be discussed in detail in the next section.

VII. HIGH INTENSITY BEAM GENERATION

Due to the unavailability of superlattice GaAs in the market, we used bulk GaAs cathodes for our beam tests. A bulk GaAs wafer was installed in a molybdenum puck with a tungsten cap covering the edge of the wafer. The GaAs wafers were activated in a preparation chamber that is connected to the gun through the cathode storage chamber. The GaAs cathodes were activated following the procedure [48]. The cathodes were atomically cleaned by heat treatment up to 580°C with a temperature ramping rate of 3°C/min. After the cathode has reached room temperature, successive deposition of Cs and O_2 can generate a typical QE of about 5% at 785 nm. The activated cathodes were transferred to the storage chamber for storage and then eventually transferred to the gun for beam extraction. All the beam tests were carried out with gun voltage at 300 kV. Two pairs of Helmholtz coils were used to compensate for the earth's magnetic field.

The laser system is a master-oscillator-power-amplifier system consisting of a commercial oscillator and an Nd-YAG, solid state rod, regenerative amplifier. The commercial oscillator operates at a constant 20 MHz, producing 1–5 ns long flattop laser pulses that get injected into the amplifier. The single stage amplifier typically runs at 10 kHz and additionally serves as pulse picker for the oscillator. The amplifier output is frequency doubled and used as pump light for an optical parametric amplifier (OPA) to amplify the output of a 785 nm laser diode to up to 130 μJ per pulse. The frequency bandwidth was measured to be 1.3 nm. This stream of typically 1.64 ns FWHM pulse length, longitudinally flattop laser pulses, after attenuation, illuminates a round aperture which is imaged through a short 5 m laser transport onto the photocathode surface in the electron gun. The transverse profile is a truncated Gaussian distribution. The laser repetition rate can be varied from 1 Hz up to 10 kHz.

We measured the bunch charge as a function of laser pulse energy to identify the space charge limit for this gun. The cathode QE was 2.7% during this measurement. The laser spot size on the cathode is 6 mm in diameter with a Gaussian sigma of 1.2 mm. The results are shown in Fig. 9. We fitted the data with 2D space charge limit model, as according to Eq. (1), which shows the space charge limit occurring at 12 nC at this beam size [49]. Note that we defined the space charge limit to be the point at which the peak of the current density Gaussian distribution starts to saturate, not as the maximum extractable bunch charge. For example, even though our gun could deliver beyond 16 nC with a 6-mm laser spot size diameter, the space charge limit is at 12 nC according to the above mentioned definition that we adopted. Our cathode size is 26 mm in diameter. Therefore, a much higher space charge limit could be achieved if we use a larger laser spot size. The EIC nominal charge 7 nC is well below the space charge limit for a 6 mm spot size.

For cathode lifetime tests, we generated 7.5 nC bunches from an area 6 mm in diameter. The beam was transported about 4.5 meters downstream to the beam dump without any measurable loss and the bunch charge was measured using the ICT at the end of the beam line. For 7.5 nC bunch charge, the beam size was 2 mm rms in diameter right before its entry into the beam dump. This measurement,

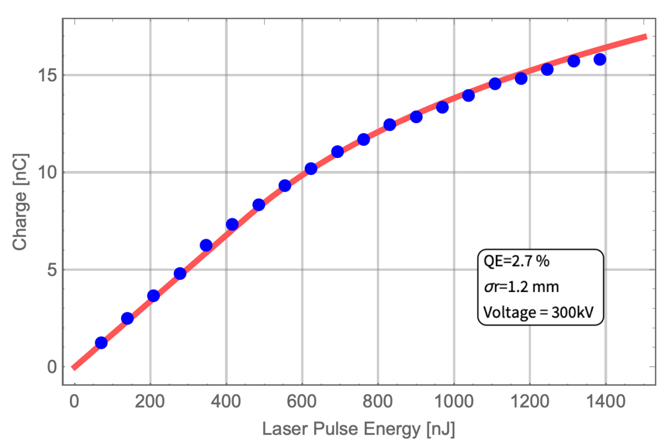

FIG. 9. Space charge limit for the EIC polarized gun with a 6 mm diameter laser spot. Blue dots are measurement and the red curve is the fitted curve.

along with radiation and vacuum levels on the beam line, indicates no beam loss in the beam transport. We performed gun beam tests for more than 100 h at various operational modes. The HVPS did not trip during this operation, showing the gun operation is very stable.

Lifetime tests were performed for various average currents—1.5, 15, 37.5, and 67.5 μA—all orders of magnitude higher than the EIC requirement. The vacuum levels on the beam line and the beam dump were measured using hot filament ULVAC AxTRAN gauges. A slow feedback system for the laser pulse energy was employed, so that the bunch charge could be kept constant while adjusting laser pulse energy. The adjustment of the laser pulse energy occurred every 15 s if the bunch charge changed by 5%. For the 1.5 and 15 μA cases, no observable QE decay was seen after 15 h of continuous operation. For the 37.5 μA operation, 10% QE decay in 9 h was observed when the anode was not biased. For this operation mode, the beamstop vacuum rose up to 7×10^{-10} Torr, whereas the beam line vacuum rose to 1.5×10^{-11} Torr. During all operations as stated so far, the cold cathode gauge in the gun vessel was below its measurement threshold. However, the cold cathode gauge can only be trustworthy down to 5×10^{-11} Torr. The gun vacuum pressure may increase to high 10^{-12} Torr to low 10^{-11} Torr scale, without the cold cathode gauge registering any reading.

Ion back bombardment was observed and determined as the main QE decay when operating at or above 10 sμA level of average currents in various facilities [50,51]. In our particular case, we have to identify whether the QE drop was due to dynamic residual gas or ion back bombardment. Therefore, we repeated the exact same experiment with the same average current, this time biasing the anode to +3 kV. Any ions generated from the beam line should be blocked by the biased anode. For the biased anode case, no observable QE decay was found over 8 h of operations. Therefore, the ions generated in the beam line dominated the QE decay when the anode was not biased. Figure 10 shows the cathode QE during operation at 37.5 μA average current, comparing the biased and unbiased anode operation modes.

The beam line is not suitable for operating high average current polarized beam without differential pumping stations, with conduction limitations, between the beam dump and the gun to intercept the back streamed gas. 67.5 μA average current operation showed clear QE decay during operation even with the anode biased. During this test, the gun vacuum would rise to 1–2×10^{-11} Torr as measured from the cold cathode gauge. The beam dump and beam line vacuum read 2×10^{-9} and 4×10^{-11} Torr, respectively. This rise in vacuum is a direct result of the rise in beamstop and beam line vacuum. An increase in the gun vacuum will increase chemical poisoning and ion back

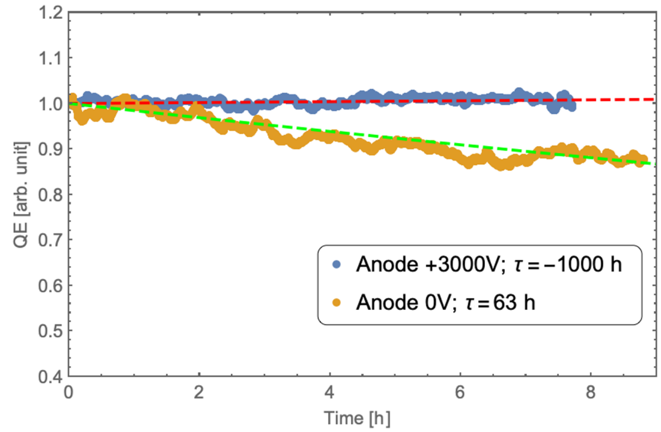

FIG. 10. Comparison of QE decay between unbiased anode and biased anode operation. The peak and average current in both cases were the same—3.5 A and 37.5 μA, respectively. The τ is the decay time using exponential fitting. The negative τ means the QE had slightly increased in 8 h.

bombardment in the dc gap. This phenomenon was clearly seen during the first beam test at 67.5 μA as 10 h of operation showed about 20% QE decay. At this point, the maximum average current and charge lifetime in this particular gun is limited by the beam dump outgassing. A short test beam line is usually not suitable to test a high current beam. In the collider, the beam dump will be kilometers away and the effects on the cathode will be negligible.

We compared the QE map before and after 67.5 μA average current operation for 39 h, as shown in Fig. 11 pie chart as 9 kHz operation. Figure 11 (left) shows different operation modes for a sample cathode using 785 nm laser. For this cathode, the majority of the operation was at 67.5 μA average current. The bunch charge was 7.5 nC for each mode, except for the QE scan. A 0.5 mm spot size was used during QE scan and extracted bunch charge was about 80 pC. The QE scans before and after the tests, as depicted by the pie chart, were shown in Fig. 11. Comparing the before and after scans, it seems that for this particular run, we did not observe the typical ion back bombardment caused sharp QE drop at the center of the cathode. From previous experiments at various facilities and simulations, a signature of ion back bombardment dominated QE decay is generally seen in major QE loss at the electrostatic center of the cathode. In our case, the decay is rather uniform over the entire activation area rather than small deep trenches in certain spots. This result indicates that chemical poisoning induced by back streamed gas could have played a key role in degrading the cathode.

We simulated the dynamic vacuum in the beam line using MolFlow+. Assuming 1×10^{-9} Torr vacuum in the beamstop, and with the existing pumping on the beam line as outlined in the previous sections, we found that the rise

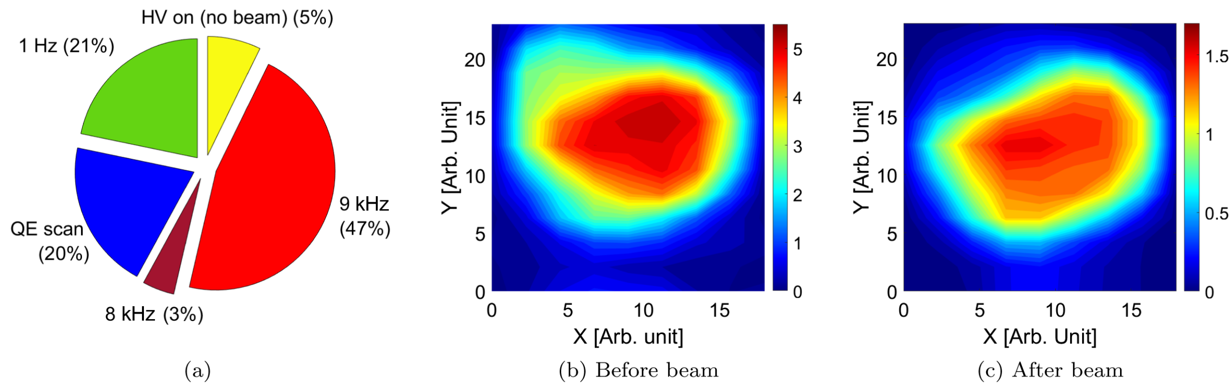

FIG. 11. Left: fractional amount of time spent on a sample cathode for different operation modes. The percents in the bracket indicate the percentage of overall operation time from this cathode. Middle: QE scan of the cathode before any beam was extracted. Right: QE scan after the cathode was used as per the left pie chart. The colorbar represents QE in percent (%). Note the scale change on the colorbar for "After beam" scan compared to "Before beam" scan.

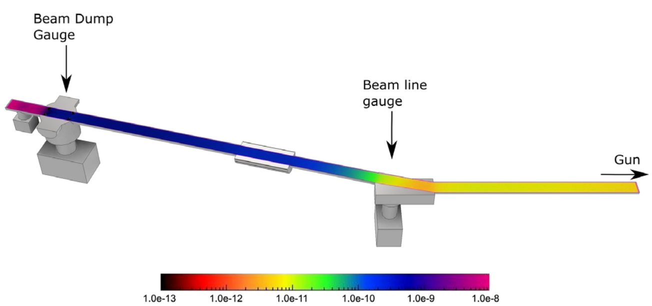

FIG. 12. MolFlow+ simulation of the beam line, assuming a 1×10^{-9} Torr vacuum in the beamstop.

in the gun vacuum to 10^{-11} Torr scale is reasonable. The results are shown in Fig. 12.

The EIC polarized electron source requirements and the beam parameters of gun achieved in stable operation are listed in Table II.

The EIC gun parameters require 0.0338 C charge to be delivered in a week. During the 37.5 μA continuous operation of 7.5 h, with no observable QE decay, we delivered approximately 30 times of EIC's weekly charge requirement. Therefore, it is accurate to say that this gun has exceeded the EIC requirements by a substantial margin.

TABLE II. EIC polarized electron source requirement and the R&D gun achieved value.

	EIC requirement	Achieved in stable operations
Gap voltage	280 kV	300 kV
Peak current	4.5 A	4.8 A
Frequency	1 Hz with eight bunches	9000 Hz
Average current	56 nA	67.5 μA
Bunch charge	7 nC	7.5 nC

Figure 13 shows a comparison between various polarized guns around the world. Other operational guns, past and present, would either have a high bunch charge (1 nC) or high average current (> tens μA) but not both. For example, CEBAF operation and R&D gun could operate in a range from 100 μA to several mA level average current but with pC level bunch charge [52]. On the other hand, SLAC and MIT guns had higher bunch charge but with relatively low average current [4]. This EIC gun is unique because it can operate in a regime where higher average currents (67.5 μA demonstrated so far) can be delivered with bunch charges in 10 nC level.

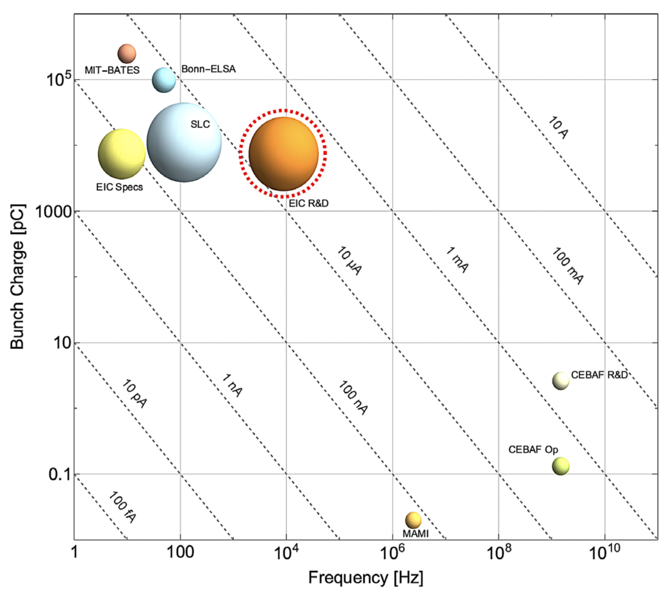

FIG. 13. Comparison of various gun from different facilities around the world. The sloped line shows the average current contour level as labeled. The ball diameter is representative of the peak current of the gun. The red dashed line at EIC R&D shows the maximum achieved peak current of 8 A.

VIII. CONCLUSION

We have designed and commissioned a HVDC polarized electron gun to meet the EIC polarized electron beam requirement. This gun employs various novel concepts, including a cathode cooling system which could be implemented in future high current electron sources. The gun was conditioned up to 350 kV without any field emission and consistently operated at 300 kV. High bunch charge, up to 16 nC, the beam was generated from bulk GaAs photocathodes using a 785 nm circularly polarized laser. Gun performance, including operational lifetime, exceeds all EIC requirements. Lifetime experiments with up to 37.5 μA level average currents, with a biased anode, show no observable QE decay over 15 h. At this point, the lifetime for 67.5 μA average current from this gun is limited by beam dump outgassing.

ACKNOWLEDGMENTS

The authors would like to acknowledge Ronald Napoli for assembling the gun and beam line. The authors would like to thank Matthew Poelker, Carlos Hernandez-Garcia, and Joe Grames from Jefferson lab for useful discussions and Don Bullard from JLab for polishing the high voltage electrode. The authors are thankful to Zachary Conway and the SRF group of Collider Accelerator Department for electrode cleaning process. The authors would like to acknowledge Charles Hetzel and NSLS II vacuum group at BNL for vacuum support. The authors would like to thank Prof. Thomas Hemmick, and Stony Brook University machine shop for their facility and technical support. Finally, the authors would like to acknowledge the following vendors with the design effort: Jerry A. Goldlust, Peter Dandridge—Dielectric Sciences; Mike Ackeret and Jason Pietz—UHV Transfer Systems; Tom Casey, Tom Beard, Richard, and Jed Bothell—Atlas Technologies; Tom Bogdan—MDC. Enrico Maccallini, and Paolo Manini—SAES Group. The work is supported by Brookhaven Science Associates, LLC under Contract No. DE-SC0012704 with the U.S. Department of Energy.

[1] H.-W. Lin, E. R. Nocera, F. Olness, K. Orginos, J. Rojo, A. Accardi, C. Alexandrou, A. Bacchetta, G. Bozzi, J.-W. Chen *et al.*, Parton distributions and lattice QCD calculations: A community white paper, Prog. Part. Nucl. Phys. **100**, 107 (2018).

[2] F. Willeke, Electron ion collider conceptual design report 2021, Report No. BNL-221006-2021-FORE, 2021, 10.2172/1765663.

[3] E. Wang, W. Liu, V. H. Ranjbar, J. Skaritka, N. Tsoupas, J. Grames, and J. Guo, The design of a high charge polarized preinjector for the electron-ion collider, in *Proceedings of the 12th International Particle Accelerator Conference, IPAC-2021, Campinas, SP, Brazil* (JACoW, Geneva, Switzerland, 2021), TUPAB037, https://jacow.org/ipac2021/papers/tupab036.pdf.

[4] J. Clendenin, Polarized electron sources, in *Proceedings of the 16th Particle Accelerator Conference, Dallas, TX, 1995* (IEEE, New York, 1995), Vol. 2, pp. 877–881.

[5] C. K. Sinclair, P. A. Adderley, B. M. Dunham, J. C. Hansknecht, P. Hartmann, M. Poelker, J. S. Price, P. M. Rutt, W. J. Schneider, and M. Steigerwald, Development of a high average current polarized electron source with long cathode operational lifetime, Phys. Rev. ST Accel. Beams **10**, 023501 (2007).

[6] J. Grames, P. Adderley, J. Brittian, J. Clark, J. Hansknecht, D. Machie, M. Poelker, M. Stutzman, R. Suleiman, and K. Surles-Law, Lifetime measurements of high polarization strained-superlattice gallium arsenide at beam current > 1 milliamp using a new 100 kV load lock photogun, in *Proceedings of the 2007 IEEE Particle Accelerator Conference, PAC-2007, Albuquerque, NM* (IEEE, New York, 2007), pp. 3130–3132.

[7] M. BastaniNejad, M. Poelker, J. McCarter, J. Hansknecht, K. Surles-Law, J. Grames, M. Stutzman, J. Clark, R. Suleiman, and P. Adderley, CEBAF 200 kV inverted electron gun, Conf. Proc. C **C110328**, 1501 (2011), https://inspirehep.net/literature/1187155.

[8] D. Schultz, R. Alley, H. Aoyagi, J. Clendenin, J. Frisch, C. Garden, E. Hoyt, R. Kirby, L. Klaisner, A. Kulikov, G. Mulhollan, C. Prescott, P. Saez, H. Tang, J. Turner, M. Woods, D. Yeremian, and M. Zolotorev, The high peak current polarized electron source of the Stanford Linear Collider, Nucl. Instrum. Methods Phys. Res., Sect. A **340**, 127 (1994).

[9] W. von Drachenfels, F. Frommberger, M. Gowin, W. Hillert, M. Hoffmann, and B. Neff, The polarized electron source at ELSA, AIP Conf. Proc. **675**, 1053 (2003).

[10] E. Tsentalovich, D. Barkhuff, J. Chen, G. Dodson, M. Farkhondeh, W. Franklin, E. Ihloff, F. Kaertner, C. Tschalaer, B. Yang, and T. Zwart, Development of a polarized electron source for the mit-bates linear accelerator center, Nucl. Instrum. Methods Phys. Res., Sect. A **582**, 413 (2007).

[11] K. Wada, M. Yamamoto, T. Nakanishi, S. Okumi, T. Gotoh, C. Suzuki, F. Furuta, T. Nishitani, M. Miyamoto, M. Kuwahara, T. Hirose, R. Mizuno, N. Yamamoto, H. Matsumoto, and M. Yoshioka, 200 keV polarized electron source at Nagoya University, AIP Conf. Proc. **675**, 1063 (2003).

[12] M. J. J. van den Putte, C. W. de Jager, S. G. Konstantinov, V. Y. Korchagin, F. B. Kroes, E. P. van Leeuwen, B. L. Militsyn, N. H. Papadakis, S. G. Popov, G. V. Serdobintsev, Y. M. Shatunov, S. V. Shevelev, T. G. B. W. Sluijk, A. S. Terekhov, and Y. F. Tokarev, The polarized electron source at NIKHEF, AIP Conf. Proc. **421**, 260 (1998).

[13] D. Abbott *et al.* (PEPPo Collaboration), Production of Highly Polarized Positrons Using Polarized Electrons at MeV Energies, Phys. Rev. Lett. **116**, 214801 (2016).

[14] P. Agostini *et al.*, The large hadron-electron collider at the HL-LHC (2021), J. Phys. G **48**, 110501 (2021)

[15] E. Wang, S. Peggs, V. Ptitsyn, F. Willeke, W. Xu, S. Benson, T. Jefferson, C. Mayes, and C. Gulliford, The accelerator design progress for EIC strong hadron cooling,

in *Proceedings of the 12th International Particle Accelerator Conference, IPAC-2021, Campinas, SP, Brazil* (JACoW, Geneva, Switzerland, 2021), pp. 1424–1427.
[16] E. Wang *et al.*, Long lifetime of bialkali photocathodes operating in high gradient superconducting radio frequency gun, Sci. Rep. **11**, 4477 (2021).
[17] S. Benson, M. Bruker, A. V. Fedotov, X. Gu, C. Gulliford, J. Guo, A. Hutton, J. Kewisch, D. Kayran, V. Ptitsyn, R. Rimmer, T. Satogata, S. Seletskiy, A. Seryi, E. Wang, H. Wang, H. Zhang, Y. Zhang, and H. Zhao, Low-energy cooling for electron ion collider, Report No. EIC-HDR-TN-012; BNL-220686-2020-TECH, 2020, 10.2172/1749902.
[18] N. Nakamura, R. Kato, H. Sakai, K. Tsuchiya, Y. Tanimoto, Y. Honda, T. Miyajima, M. Shimada, T. Obina, and H. Kawata, Demonstration of proof of concept of the EUV-FEL for future lithography, in *Proceedings of the International Conference on Extreme Ultraviolet Lithography 2021*, edited by K. G. Ronse, P. P. Naulleau, P. A. Gargini, T. Itani, and E. Hendrickx, International Society for Optics and Photonics Vol. 11854 (SPIE, 2021), 10.1117/12.2600782.
[19] D. T. Pierce and F. Meier, Photoemission of spin-polarized electrons from GaAs, Phys. Rev. B **13**, 5484 (1976).
[20] D. Durek, F. Frommberger, T. Reichelt, and M. Westermann, Degradation of a gallium-arsenide photoemitting NEA surface by water vapour, Appl. Surf. Sci. **143**, 319 (1999).
[21] F. Machuca, Z. Liu, Y. Sun, P. Pianetta, W. Spicer, and R. Pease, Role of oxygen in semiconductor negative electron affinity photocathodes, J. Vac. Sci. Technol. B **20**, 2721 (2002).
[22] E. Wang, I. Ben-Zvi, R. Lambiase, W. Liu, O. Rahman, J. Skaritka, and F. Willeke, The progress of high current high bunch charge polarized electron HVDC gun, in *Proceedings of the 10th International Particle Accelerator Conference, IPAC-2019, Melbourne, Australia* (JACoW, Geneva, Switzerland, 2019), TUPTS103, 10.18429/JACoW-IPAC2019-TUPTS103.
[23] J. M. Grames, P. A. Adderley, J. C. Hansknecht, M. Poelker, D. G. Moser, M. L. Stutzman, and S. Zhang, Milliampere beam studies using high polarization photocathodes at the CEBAF photoinjector, Proc. Sci., PSTP2017 (324) (**2018**) 016, 10.22323/1.324.0014.
[24] J. Grames, P. Adderley, J. Brittian, J. Clark, J. Hansknecht, D. Machie, M. Poelker, E. Pozdeyev, M. Stutzman, and K. Surles-Law, A biased anode to suppress ion back-bombardment in a dc high voltage photoelectron gun, AIP Conf. Proc. **980**, 110 (2008).
[25] E. Pozdeyev, Ion trapping and cathode bombardment by trapped ions in dc photoguns, Phys. Rev. ST Accel. Beams **10**, 083501 (2007).
[26] O. Rahman, E. Wang, I. Ben-Zvi, J. Biswas, and J. Skaritka, Increasing charge lifetime in dc polarized electron guns by offsetting the anode, Phys. Rev. Accel. Beams **22**, 083401 (2019).
[27] K. Aulenbacher, V. Tioukine, M. Wiessner, and K. Winkler, Status of the polarized source at MAMI, AIP Conf. Proc. **675**, 1088 (2003).
[28] J. Grames, R. Suleiman, P. A. Adderley, J. Clark, J. Hansknecht, D. Machie, M. Poelker, and M. L. Stutzman, Charge and fluence lifetime measurements of a dc high voltage GaAs photogun at high average current, Phys. Rev. ST Accel. Beams **14**, 043501 (2011).
[29] C. Hernandez-Garcia *et al.*, Compact −300 kV dc inverted insulator photogun with biased anode and alkali-antimonide photocathode, Phys. Rev. Accel. Beams **22**, 113401 (2019).
[30] T. Siggins, C. Sinclair, C. Bohn, D. Bullard, D. Douglas, A. Grippo, J. Gubeli, G. Krafft, and B. Yunn, Performance of a dc GaAs photocathode gun for the Jefferson Lab FEL, Nucl. Instrum. Methods Phys. Res., Sect. A **475**, 549 (2001).
[31] Y. Y. Lau, Simple Theory for the Two-dimensional Child-Langmuir Law, Phys. Rev. Lett. **87**, 278301 (2001).
[32] SCT ceramics, https://www.sct-ceramics.com/en/.
[33] G. Mulhollan, A. Subashiev, J. Clendenin, E. Garwin, R. Kirby, T. Maruyama, and R. Prepost, Photovoltage effects in photoemission from thin GaAs layers, Phys. Lett. A **282**, 309 (2001).
[34] T. Maruyama, A. Brachmann, J. Clendenin, T. Desikan, E. Garwin, R. Kirby, D.-A. Luh, J. Turner, and R. Prepost, A very high charge, high polarization gradient-doped strained GaAs photocathode, Nucl. Instrum. Methods Phys. Res., Sect. A **492**, 199 (2002).
[35] C. Hernandez-Garcia, M. Poelker, and J. Hansknecht, High voltage studies of inverted-geometry ceramic insulators for a 350 kV dc polarized electron gun, IEEE Trans. Dielectr. Electr. Insul. **23**, 418 (2016).
[36] V. F. Software, OPERA3D simulation software, https://www.3ds.com/products-services/simulia/products/opera/.
[37] Los Alamos Accelerator Code Group, POISSON SUPERFISH, https://laacg.lanl.gov/laacg/services/download_sf.phtml.
[38] C. Hernandez-Garcia, D. Bullard, F. Hannon, Y. Wang, and M. Poelker, High voltage performance of a dc photoemission electron gun with centrifugal barrel-polished electrodes, Rev. Sci. Instrum. **88**, 093303 (2017).
[39] X. Gu *et al.*, Stable operation of a high-voltage high-current dc photoemission gun for the bunched beam electron cooler in RHIC, Phys. Rev. Accel. Beams **23**, 013401 (2020).
[40] N. Nishimori, R. Nagai, R. Hajima, M. Yamamoto, Y. Honda, T. Miyajima, and T. Uchiyama, Operational experience of a 500 kV photoemission gun, Phys. Rev. Accel. Beams **22**, 053402 (2019).
[41] E. Wang, High current polarized electron source for future eRHIC, AIP Conf. Proc. **1970**, 050008 (2018).
[42] E. Tsentalovich, J. Bessuille, E. Ihloff, J. Kelsey, R. Redwine, and C. Vidal, High intensity polarized electron source, Nucl. Instrum. Methods Phys. Res., Sect. A **947**, 162734 (2019).
[43] E. P. T. Robert P. Redwine, High intensity polarized electron gun, Technical Report, MIT Bates Linear Accelerator Center, 2015, https://dspace.mit.edu/bitstream/handle/1721.1/102631/DOE_FY16_pol_el-160425.pdf?sequence=1; Later they published a tech-report https://www.osti.gov/biblio/1481409.
[44] M. Gaowei, E. Wang, J. Cen, A. Fedotov, D. Kayran, R. Lehn, C. J. Liaw, T. Rao, J. Tuozzolo, and J. Walsh, High

current performance of alkali antimonide photocathode in LEReC DC gun, in *Proceedings of the 63rd ICFA Advanced Beam Dynamics Workshop on Energy Recovery Linacs, ERL2019* (JACoW, Berlin, Germany, 2019).

[45] Saes group, https://www.saesgetters.com/products/zao-wafer-modules.

[46] R. Kersevan and J.-L. Pons, Introduction to MolFlow+: New graphical processing unit-based Monte Carlo code for simulating molecular flows and for calculating angular coefficients in the compute unified device architecture environment, J. Vac. Sci. Technol. A **27**, 1017 (2009).

[47] F. Watanabe, Bent belt-beam gauge: Extending low-pressure measurement limits in a hot-cathode ionization vacuum gauge by combining multiple methods, J. Vac. Sci. Technol. A **28**, 486 (2010).

[48] J. Biswas, J. Cen, M. Gaowei, O. Rahman, W. Liu, X. Tong, and E. Wang, Revisiting heat treatment and surface activation of GaAs photocathodes: In situ studies using scanning tunneling microscopy and photoelectron spectroscopy, J. Appl. Phys. **128**, 045308 (2020).

[49] S. Hartman, N. Barov, C. Pellegrini, S. Park, J. Rosenzweig, G. Travish, R. Zhang, C. Clayton, P. Davis, M. Everett, C. Joshi, and G. Hairapetian, Initial measurements of the UCLA rf photoinjector, Nucl. Instrum. Methods Phys. Res., Sect. A **340**, 219 (1994).

[50] J. Grames, P. Adderley, J. Brittian, J. Clark, J. Hansknecht, D. Machie, M. Poelker, E. Pozdeyev, M. Stutzman, and K. Surles-Law, A biased anode to suppress ion back-bombardment in a dc high voltage photoelectron gun, AIP Conf. Proc. **980**, 110 (2008).

[51] W. Liu, S. Zhang, M. Stutzman, and M. Poelker, Effects of ion bombardment on bulk GaAs photocathodes with different surface-cleavage planes, Phys. Rev. Accel. Beams **19**, 103402 (2016).

[52] P. Adderley, J. Clark, J. Grames, J. Hansknecht, M. Poelker, M. Stutzman, R. Suleiman, K. Surles-Law, J. McCarter, and M. BastaniNejad, CEBAF 200 kV inverted electron gun, in *Proceedings of the 2011 Particle Accelerator Conference, PAC-2011, New York, 2011* (IEEE, New York, 2011), pp. 1501–1503.